Available online at www.sciencedirect.com
SCIENCE DIRECT®
Geochimical
ELSEVIER
Geochimica et Cosmochimica Acta 70 (2006) 3582-3592
www.elsevier.com/locate/gca

The mechanisms of reduction of hexavalent chromium by green rust sodium sulphate: Formation of Cr-goethite

L.L. Skovbjerg [a,*], S.L.S. Stipp [a], S. Utsunomiya [b], R.C. Ewing [b]

[a] *NanoGeoScience Group, Geological Institute, University of Copenhagen, 0ster Voldgade 10, 1350 Copenhagen K, Denmark*
[b] *Department of Geological Sciences, The University of Michigan, 2534 C.C. Little Building, 1100 N. University Ave., Ann Arbor, MI 48109-1005, USA*

Received 12 August 2005; accepted in revised form 20 February 2006

Abstract

The molecular-level processes that control green rust sodium sulphate (GR_{Na},so_4) reaction with chromate were studied using high-resolution techniques. Changes in solid morphology, structure and composition were observed with atomic force microscopy, transmission electron microscopy and X-ray diffraction. The results suggest the following mechanisms: Chromate replaces sulphate in the GR interlayer and is reduced by Fe(II). Formation of sparingly soluble Cr(III)-solid blocks further chromate entry, but Cr(VI) reduction continues at the GR solid/solution interface. Electron transfer from the centre of the GR crystals to the surface facilitates rapid reaction. Less stable zones of the reacted GR_{Na},so_4 dissolve and amorphous Cr(HI),Fe(III)-solid forms. During equilibration, Cr-substituted goethite evolves in association with remaining GR_{N}a,so_4. fed by material from the amorphous phase and dissolving oxidised GR. In contrast, previous Cr(VI) experiments with the carbonate form of GR, GR_{C}o,» have suggested only reaction and deposition at the surface. From the perspective of environmental protection, these results have important implications. Goethite is sparingly soluble and the inclusion of Cr(III) as a solid-solution makes it even less soluble. Compared to Cr adsorbed at the surface of an Fe(III)-phase, Cr(III) incorporated in goethite is much less likely to be released back to groundwater.

1. Introduction

Hexavalent chromium is toxic, carcinogenic, probably mutagenic and highly soluble. It is released to the environment as a result of industrial products manufacturing and processes such as metal surface treatment, wood impregnation, pigments in paints and plastics and leather tanning. Chromium displays several oxidation states from 0 to +6 but of these, Cr(III) and Cr(VI) are by far most common in nature. Cr(III) is much less soluble, is considered non-toxic and serves as an important trace element in sugar metabolism (Barceloux, 1999). In Cr(VI)-polluted groundwater and soil, reduction of Cr(VI) to Cr(III) is therefore desirable. Over a wide range of conditions and especially in natural and engineered environments, effective reductants are zero-valent iron (Fe(0)), aqueous Fe^{2+} and structurally bound Fe(II) in minerals.

The term green rust (GR) refers to a series of compounds that belong to the layered double hydroxide (LDH) family. The green rust compounds are composed of positively charged Fe(II)-Fe(III) hydroxide sheets that alternate with interlayers of water molecules and anions, such as SO_4^{2}-, CO_3^{2}~ and Cl~ (Feitknecht and Keller, 1950; Bernal et al., 1959). The newest revised formula that has been published for $GR_{S}o_4$ is $Fe(II)4Fe(III)_2(OH)_{12}$. SO_4-$8H_2O$ (Simon et al., 2003). GR is stable at pH above 6 but destabilises at very high pH (Lewis, 1997) and under oxidising conditions. Green rust is thought to be common in anoxic groundwater and has been identified as a corrosion product in zero-valent iron reactive barriers (Roh et al., 2000; Wilkin et al., 2005). An iron barrier often consists of a mixture of clay, sand and a few percent of finely ground scrap iron that is deposited in the ground in a

Corresponding author.
E-mail addresses: Lskovbjerg@geol.ku.dk (L.L. Skovbjerg), stipp@**geol.ku.dk (S.L.S. Stipp),** utu@umich.edu (S. Utsunomiya), rodewing@**umich.edu (R.C.** Ewing).

0016-7037/$ - see front matter © 2006 Elsevier Inc. **All** rights reserved.
doi:10.1016/j.gca.2006.02.017

trench, dug perpendicular to a migrating plume. Some redox active contaminants are reduced by the metallic iron and immobilised, thereby decreasing bioavailability. A good introduction to the environmental applications of GR can be found in Hansen (2001).

Green rust compounds are usually classified based on the interlayer anion, but recent research indicates that monovalent cations are a necessary part of the interlayer structure for stability (Christiansen et al., 2004). The steric nature of the interlayer anion and cation affects the stacking of the hydroxide layers and results in different GR crystal structures. Two main types have been recognised. GR1, to which GR chloride (GR_a) and carbonate ($GR_{C}o_3$) belong, has a basal plane spacing of about 8 A, whereas GR2, to which GR sodium sulphate ($GR_{N}a,so_4$) is assigned, has a basal plane spacing of about 11 A (Bernal et al., 1959). The iron-hydroxide layers in LDH's are about 2 A thick (Drits and Bookin, 2001). In GR1 and GR2, this leaves about 6 and 9 A of interlayer space, which is occupied by weakly bonded cations, anions and water. The loose structure allows exchange of components from solution, including oxidants. The interlayer region provides rapid access to Fe(II) in the bulk structure and consequently, fast reduction rates.

During recent years, experimental interest has focused on green rust because of its ability to reduce several oxidised compounds that are problematic in nature such as NO_2" (Hansen et al., 1994), NO_3" (Hansen, 2001), Se(VI) (Myneni et al., 1997), U(VI) (O'Loughlin et al., 2003), Tc(VII) (Pepper et al., 2003), trichloroethylene (TCE) (Lee and Batchelor, 2002) and also Cr(VI) (Loyaux-Lawniczak et al., 1999; Loyaux-Lawniczak et al., 2000; Williams and Scherer, 2001; Bond and Fendorf, 2003; Legrand et al., 2004). The reduction of Cr(VI) by GR has been demonstrated by several researchers, often with focus on reduction rates. Although there is general agreement about the order of magnitude of the reaction rate, reports on end products and mechanisms are conflicting. Discrepancies may arise from differences in experimental setup and may be compounded further by assuming that all forms of GR behave similarly.

Bond and Fendorf (2003) compared the reduction rates of $GRso_4$, $GR_{C}o_3$ and GR_a and proposed one model for all three, which may not be appropriate because of differences in their crystal structure. Furthermore, Bond and Fendorf (2003) did not account for the differences in Fe(II) content in their three systems, which resulted from normalising by mass rather than by mole equivalents of Fe(II) as the active reducing agent. Williams and Scherer (2001) and Legrand et al. (2004) investigated Cr(VI) reduction by $GRco_3$- Both groups found that at low Cr(VI) concentrations, reduction rate was proportional to green rust surface area, but at higher concentrations, reaction rate became more complex. Legrand et al. (2004) proposed a heterogeneous reaction mechanism where successive Cr(III) monolayers precipitate on the surface of reacting $GRco_3$• This model could explain the early, very fast reduction rate and then a prolonged period (~16h) before Cr(VI) decreased below detection.

The application of different procedures for treatment of green rust after synthesis, during characterisation, storage „ and experiments is a likely cause of inconsistent results among the previous studies. Common practice is to wash freshly synthesised material with deionised water but this takes it out of equilibrium with its solution. GR responds by spontaneously decomposing to iron oxides such as magnetite. Thus, experiments made with rinsed material probably incorporate artefacts from a solid that is not at equilibrium with its solution and possibly unexpected solid phases have formed. Some researchers also freeze-dry the GR before experiments to determine the amount of starting material by weight. However, Lewis (1997) showed that drying dehydrates the interlayer, producing a different molar mass and ultimately, an unknown quantity of active Fe(II). The exchangeability of oxidants is also likely to decrease upon dehydration. Finally, some researchers add organic buffers to keep pH constant during redox reactions. The tendency for organic compounds to modify system behaviour is well known. Therefore, to better simulate natural conditions and minimise artefacts from sample handling, freshly prepared GR_{Na},s_{O4}, that had never been washed or dried, was used in all experiments. Furthermore, no extraneous compounds were added at any time during synthesis of the green rust or during any of the experiments.

In the present study, high-resolution techniques were applied to define the molecular-scale mechanisms controlling Cr(VI) reduction by GR_{Na},so_4- The interim and end products were investigated using atomic force microscopy (AFM), capillary tube X-ray diffraction (CT-XRD) and transmission electron microscopy (TEM). Our goal was to understand the mechanisms controlling the reaction. This knowledge is a key for improving reactive barrier technology.

2. Experimental details

2.1. GR_{Na,SO_4} synthesis

All GR_{Na,SO_4} was synthesised inside a plastic-walled glove box (manufactured by Coy Laboratory Products, Inc.) with internal volume of about 3 m^3. The atmosphere consisted of about 98% N_2 and 2% H_2 (gas supplied by Hydro Norway). Oxygen in the chamber was maintained at below 0.5 ppm by reaction with H_2 on a palladium catalyst. Produced water was then adsorbed on porous aluminium oxide. Our material was always stored in closed containers but the atmosphere of the glove box is anoxic enough that GR suspensions left uncapped and stirring, remain dark green, even after a full day.

Glassware used for synthesis and storage was treated with 20% HC1 and 1% HNO_3 and rinsed many times to remove Fe-oxides from previous.experiments. The initial

Fe-solution was prepared with MilliQ water (resistivity <0.1 uS/cm) deoxygenated by bubbling with 99.999% N_2 (supplied by Hydro Norway) and from commercially available melanterite ($FeSO_4$-$7H_2O$, with purity 99.5%, supplied by AppliChem). Mossbauer spectroscopy analysis of samples of dry starting material showed no detectable Fe(III) (detection limit ~2%). The initial solution, 0.05 M $FeSO_4$, had pH of 3.7. Under these conditions, the rate of oxidation of Fe(II) to Fe(III) is very low (Singer and Stumm, 1970) so the initial Fe(III) concentration was assumed to be negligible.

The use of glass for GR synthesis may be problematic, if the purpose is to determine the rate of reaction in the pure system. Hendriksen (2003) demonstrated that dissolved silica inhibits GR reactivity. EDS analysis of the GR synthesised for the experiments described here showed Si concentrations of about 2-3 wt% in pure GR crystals. Still, our samples reacted slightly faster than those reported in the literature. Because our purpose is not to determine precise reaction rates but rather mechanism, the presence of trace silica was accepted. Finally, in nature, Si is omnipresent, in clay, sand and water, so perhaps experiments in the presence of Si are more meaningful than truly ideal conditions.

For GR_{Na},so_4 synthesis, 200 mL of the 0.05 M $FeSO_4$ solution was oxidised in a 250-mL open glass beaker (inside the glove box) with fast stirring by a Teflon coated, magnetic stirring bar at room temperature. NaOH was added drop-wise to maintain pH at 7 (±0.2). The solution was oxidised slowly by O_2 added as ambient air. The air was conducted into the glove box and through the solution via a thin plastic tube. A peristaltic pump controlled air bubbling speed. To avoid formation of GR_Co_3, CO_2 was removed from the air by bubbling it through a 20% NaOH solution. The GR synthesis method was modified from that described by Koch and Hansen (1997) to fit the conditions in our laboratory.

During oxygen addition, 1 M NaOH (standard titration solution from Merck) was added with a pH-stat (supplied by Radiometer) at a rate usually varying from 0.04 to 0.09 mL/min, to a total of about 16 mL. Eh, measured with an Ag/Ag^+ platinum electrode was monitored continuously. During GR synthesis, Eh is rather stable, usually between -0.5 and -0.3 mV. The solution equilibrates with the glove box atmosphere, so H_2 has an effect on composition, but it has been assumed to be inconsequential for the preparation of the solid or the mechanisms by which it reacts. When the solution became depleted in Fe^{2+}, Eh began to rise and oxidation was halted. The suspension was not oxidised until Fe^{2+} was exhausted because a solution without Fe^{2+} would destabilise GR. Instead, the remaining aqueous Fe^{2+} (Fe^{2+}_{end}) was determined and used to estimate the amount of Fe(II) that had been precipitated as GRNaso$_4$ by mass balance. Fe(II) in the solid is represented by

$$\mathrm{Fe(II)}_{\mathrm{GR_{Na,SO_4}}} = \tfrac{4}{6}(\mathrm{Fe^{2+}}_{\mathrm{initial}} - \mathrm{Fe^{2+}}_{\mathrm{end}}), \quad (1)$$

where $Fe^{2+}_{init}i_ai$ denotes the molar concentration of added $FeSO_4$-$7H_2O$. The ratio 4/6 is the Fe(II)/(Fe(II) + Fe(III)) ratio for GR_So_4 (Bernal et al., 1959; Hansen et al., 1994; Simon et al., 2003).

To minimise the risk of altering the composition and structure of green rust, drying of the solids was avoided. Instead, a method was developed to make aliquots of the original GR suspension, where the quantity of solid could be determined accurately. The method was tested by measuring out a set of suspension aliquots by volume and then weighing them after drying. These samples were not used for experiments. Reproducibility of the GR mass in the portion pipetted out by this method was about 5%. Thus, the GR suspensions intended for experiments were divided into aliquots; some were used for characterisation and the rest, for reaction with Cr(VI).

2.2. Reaction between chromate and GRN_O,SO_4

The number of moles of Cr(VI) added to each of the experiments was defined by the percentage of Fe(II) in the GR that would be oxidised by the Cr(VI). We define the parameter, Oxc$_r$(vi)/Fe(ii)(%)> to show the ratio of Cr(VI) available to Fe(II) from GR that can serve as an electron donor. When $Ox_{Cr(V}$i)/Fe(ii) < 100%, Fe(II) in GR is in excess and when Ox_{Cr}(vi)/Fe(ii) > 100%, more Cr(VI) is present than can be reduced by the GR in suspension. Some of the added Cr(VI) is reduced by ferrous iron present in the equilibrium supernatant. This amount, which is taken as the difference between Fe^{2+} measured at t = 0 (before addition) and 5 min later (when the measured concentration of $Fe^{2+}_{(aq)}$ was at a minimum; Table 1), is subtracted from the quantity of Cr added so that Ox_{Cr}(vi)/Fe(ii) indicates more accurately how much of the GR is oxidized.

Chromate was added as solutions of K_2Cr0_4 (99.5% pure, supplied by Merck) to suspensions of $GR_{Na}So_4$ that had never been dried or rinsed. The pH of the chromate solutions were about 9.2. Concentrations were chosen to provide low (L), medium (M), high *(H)* and very high *(VH)* ratios for Cr(VI) available, relative to Fe(II) present in the green rust (Table 1). The suspensions were then left stirring in the glove box at room temperature and sampled frequently (4 or 5 times) during the first 10 days and *(VH)* also after 18 years to examine evolution of atomic structure, morphology and chemical composition. K_2Cr0_4 was chosen as the chromate salt in order to compare to previous work on Cr(VI) reduction by GR (Williams and Scherer, 2001; Bond and Fendorf, 2003). The resulting K^+/Na^+ ratio in suspension was less than 2%. K^+ from the chromate solutions may substitute for Na^+ in the GRNa,so_4 structure and affect the results, but recent research in our group (Christiansen et al., unpublished results) shows that green rust potassium sulphate, GRKSO_4> has a very similar structure. Thus, it is assumed that K^+ has a negligible effect on the solid-state transformation mechanisms.

Table 1
Experimental details

Batch	$Ox_{Cr<VI)/Fe(II)}$ (%)	Cr(VI) solutions added (mol/L)	Sampling time	Fe(II) in GR (mM)	Fe(II) in supernatant (ppm)	Cr(VI) in supernatant (ppm)	Total Cr in supernatant (ppm)	High-resolution technique
Low Cr concentration (L)	5	1.3 mL of 0.1 M K_2CrO_4 to 166 mL GR suspension	0 5 min 30min 4.5 h 24 h	30.1	270 226 234 260 252	0		AFM, XRD
Medium Cr concentration *(M)*	~35	1.4mLof0.3M K_2Cr0_4 to 95 mL GR suspension	0 10 min 5 days 10 days	31.4	160			TEM
	32	0.9 mL of 0.8 M K_2CrO_4 to 166 mL GR suspension	0 5 min 30 min 4.5 h 24 h	31.1	190 25 38 80 116	0		AFM, XRD '
High Cr concentration *(H)*	~72	2.7mLof0.3M K_2Cr0_4 to 95 mL GR suspension	0 10 min 20 h 6 days	31.4	160			TEM, AFM[a], XRD[a]
	66	1.7mLof 0.8 M $K_2CrO_4$to 167 mL GR suspension	0 5 min 30 min 4.5 h 24 h 5 days	30.5	240 <1 19 24	0	0 0 0 0	AFM
Very high Cr concentration *(VH)*	110	2.6 mL of 0.8 M K_2CrO_4 to 166 mL GR suspension	0 5 min 30 min 4.5 h 24 h 1.8 years	31.2	175 0 0 0 0	235 173 82	292 204 98 94	AFM, XRD

Concentrations of Cr(VI) added and sampling times.
[a] Results collected from stock GR where no Cr had been added.

The solid was separated from the solution using 0.2 um cellulose acetate filters (from Sartorius). Samples of the solutions were sealed in test tubes to minimize oxidation during transport from the glove box to immediate elemental analysis. Fe(II) and Cr(VI) concentrations were determined with a Perkin-Elmer 55E spectrophotometer using the ferrozine (Gibbs, 1976) and diphenylcarbazide methods (APHA, AWWA and WPCF, 1975). Total Fe and total Cr were analysed using a Perkin-Elmer 5100 atomic absorption spectrometer (AAS).

The solid filter cake was dried on the membrane inside the glove box. Samples for XRD were prepared by crushing the material with tweezers in a plastic cup or by grinding in a folded piece of paper. To avoid oxidation, the powder was then transferred to quartz glass capillary tubes (CT) (diameter 0.4 mm) and sealed with paraffin before removal from the glove box. No colour change and no modification in the XRD pattern were observed, even when the sealed tube was exposed to air for several days. The XRD instrument was a Bruker AXS four-circle diffractometer, equipped with a molybdenum source and a graphite filter.

Samples for AFM were made from a droplet of suspension deposited on freshly cleaved mica, at the same time and from the same batches as samples for chemical analysis and XRD. Images were taken on a Digital Multimode Ilia, operating in contact force mode and using standard SisN4 tips. The entire microscope was installed inside the glove box, to minimise risk of oxidation.

TEM was done on separate batches of GR suspension that had been prepared by the same method. TEM samples were prepared in an N_2 atmosphere glove bag (volume ~0.6 m^3). A droplet of GR suspension was deposited on a Cu-TEM grid with holey carbon mesh and after 5 s, loose material was flushed away with demineralised water. After drying for 15-30 min in the glove bag, the samples were placed in small plastic containers, sealed with parafilm and transported to the TEM instrument within about 5 min. Transfer from the plastic container to the TEM sample holder, in air, took less than a minute. Pressure in the TEM chamber was 1.5 x 10^{-7} torr. Although the samples were exposed to air for nearly

a minute, tests have shown that when samples are dry, they can be exposed to air for many hours before the effects of oxidation can be recognised. Thus, negligible effects from the sample procedure on interpretation of the reaction mechanism were assumed.

The TEM instrument was a JEOL 201 OF with Fas-TEM system and a Gatan Imaging Filter (GIF) located at Electron Micro-beam Analysis Laboratory (EMAL) at University of Michigan. TEM images were acquired using Gatan Digital Micrograph, version 3.6.4. Bright-field TEM (BF-TEM), High-angle annular dark field scanning TEM (HAADF-STEM), high-resolution TEM (HR-TEM), energy dispersive X-ray spectrometry (EDS) and selected area electron diffraction (SAED) analysis were conducted. The microscope was operated at an acceleration voltage of 200 kV, produced from a zirconated tungsten (100) thermal field emission tip. Cs is 1.0 mm. The spatial resolution was 0.10 nm of lattice resolution and 0.25 nm for point-to-point resolution in TEM mode and 0.17 nm for lattice resolution in scanning TEM (STEM) mode. In HAADF-STEM, the probe size was 0.5 nm. The EDS system had an EDAX r-TEM detector with EDAX Genesis software. The detector was an ultra-thin window Si-Li X-ray detector, which can analyze all elements with $Z > 5$. The EDS spectra were produced by rastering the beam in STEM mode with a lOxlOnm, 15xl5nm or 30x30nm beam to minimise damage by the electron beam. Acquisition time of EDS analysis was in all cases longer than 90 s.

3. **Results and discussion**

3.1. Characterisation of GR_{Na,SO_4}

The $GR_{Nais}o_4$ starting material was characterised with CT-XRD, AFM and TEM. XRD patterns (Fig. la) compare well with previous results (Bernal et al., 1959; Hansen et al., 1994; Simon et al., 2003) except that finer detail and some additional lines are revealed with the capillary tube (CT) method (Christiansen et al., 2004). TEM and AFM (Figs, lb and c) demonstrated plate-like individual crystals with a sharp hexagonal outline, 10-35 nm thick with crystal diameter ranging from 1 to 2 nm to less than 100 nm. Most crystals are uniform and flat on the basal plane. Some GR grains reveal terraces that are only one or a few monolayers high. The morphology is consistent with previously published images of $GR_{Nais}o_4$ (Gehin et al., 2002).

The fresh GR batches used for most experiments contained no other identifiable phases. Those used for the TEM investigations were synthesised fresh, immediately before travel to the TEM facility. XRD and AFM results from these did not indicate the presence of solids other than $GR_{Nais}o_4$ but samples analysed with TEM 11 days after synthesis showed trace quantities of small magnetite crystals (diameter about 100-250 nm). When samples from the same suspensions were analysed with XRD seven weeks later, the presence of trace quantities of magnetite was verified. Magnetite is a common GR oxidation product. The TEM batches were synthesised with a higher oxidation rate; base addition rate was 0.12mL/min rather than the 0.04-0.09 mL/min used for the other batches and it had been stored 11 days in a sealed glass bottle, out of the glove box during transport, before the TEM investigations began. Magnetite particles may initially have been too small or too few for the 2% XRD detection limit, but they may have grown in size or proportion during the intervening seven weeks. Because a small amount of the Fe in the system crystallised as magnetite, a fraction less was available as GR for reaction with Cr(VI). However, the concentration of magnetite was very low, and the purpose of this study was to determine the GR transformation mechanism, not the rate, so it is a safe assumption that trace magnetite in the TEM batch had no effect on the results. This is supported by consistent results from TEM and the other experiments.

3.2. Cr(VI) reaction and characterisation of the end products

The transformation of GRN_aso_4 from a ferrous-ferric to a ferric compound by oxidation with Cr(VI) was monitored as a function of time after adding chromate. Experiment details are summarised in Table 1. In cases where enough Fe(II) was present in suspension to reduce all Cr(VI) and where more than 30% of the Fe(II) in suspension remained unoxidised *(L, M* and *H),* Cr(VI) concentration in solution dropped to background within 5 min of addition. But when Ox_{Cr}(vi)/Fe(ii) $>$ 100% (*VH),* the reaction rate decreased significantly. The reaction rates determined for Ox_{Cr}(vi)/Fe(ii) < 100% are slightly faster than rates reported by Williams and Scherer (2001), Bond and Fendorf (2003), and Legrand et al. (2004) for $GR_{S}o_4$ and $GRco_3$- Our experiments used fresh GR in its supernatant, without rinsing with deionised water and without drying. Aside from the effect of interlayer ions (namely SO_4^{2}~, CO_3^{2}~ and Cl~), the different treatment of the initial GR is probably responsible for the faster reaction rate observed here.

Cr(VI) was added to the green rust in suspensions at equilibrium with the supernatant. Therefore, the solution contained dissolved Fe^{2+}, which was also available for reaction with Cr(VI). Williams and Scherer (2001) suggested that Fe(II) in GR reacts more readily than aqueous Fe^{2+}. However, the rates may be comparable when both are present in the suspension. This was confirmed in one of our experiments where Cr(VI) concentration was very low and enough Fe^{2+} was present in solution to reduce all of it. Reduction happened very fast and morphological changes in the GR crystals, observed with AFM, provided clear evidence of oxidation (images not shown), but the concentration of dissolved Fe^{2+} also decreased (Table 1). This suggests that $Fe^{2+}{}_{(aq)}$ was oxidised by Cr(VI) with GR acting as a reaction substrate, thereby enhancing the rate of reaction. To perform an experiment with only supernatant, with the goal of defining the contribution

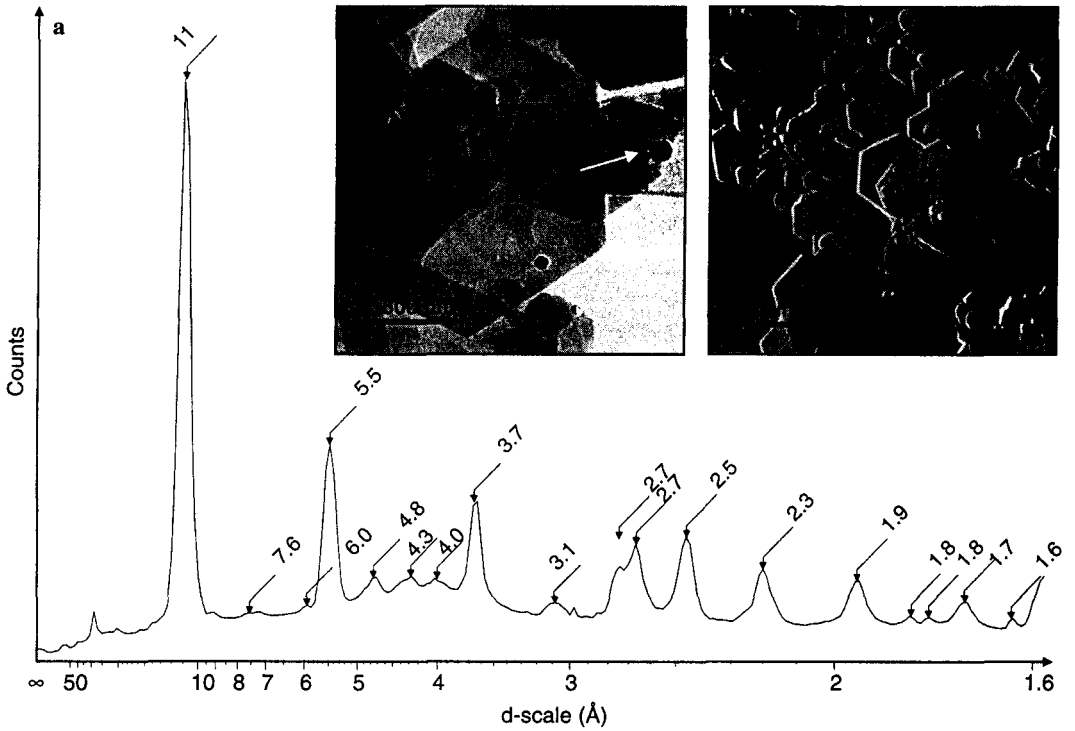

Fig. 1. Fresh GR_{NaSO_4} before reaction with Cr(VI). (a) XRD reveals the GR2 structure with basal spacing of about 11 A. No other phases are visible, (b) TEM image. The small black crystals (arrow) are magnetite, (c) AFM image. Most crystals are uniformly flat; some have small steps as **on the large crystal** in the lower left corner.

from aqueous ferrous iron alone, in the absence of GR, is likely to prove difficult. At pH 7, any ferric iron formed by reduction of chromium will combine with the remaining ferrous iron and form GR, which can then react and act as a reaction substrate. The evolution of dissolved iron concentration was monitored during most experiments (Table 1) and was incorporated in the interpretations.

XRD shows the overall structural evolution of the material. Fig. 2 presents patterns after reaction in solutions where $Ox_{Cr(VI)/Fe(II)} = 66\%$. First, an amorphous phase with broad peaks in the goethite regions is produced. Crystallinity gradually increases over several days, which is consistent with TEM results. TEM and semi-quantitative EDS analysis revealed that poorly crystalline material formed, with Cr/(Cr + Fe) ratios of 25% and 37% in suspensions $M_{10\,min}$ and $H_{10\,min}$. Goethite that formed subsequently in the same samples, as well as the remaining GR, was associated with less Cr (on average 5% and 9% Cr/(Cr + Fe) in suspensions $M_{\geqslant 20\,h}$ and $H_{\geqslant 20\,h}$). This 5 to 10% is more, however, than can be explained simply by adsorption on goethite surfaces. Both the poorly crystalline material and the remaining GR dissolved almost completely after a few days when Cr(VI) concentration was high but the fraction of Cr associated with goethite did not change with time or with the extent of reaction. Because there was no detectable Cr in the supernatant, it can be interpreted that Cr was captured, either by adsorption or incorporation into the structure of the oxidised phases.

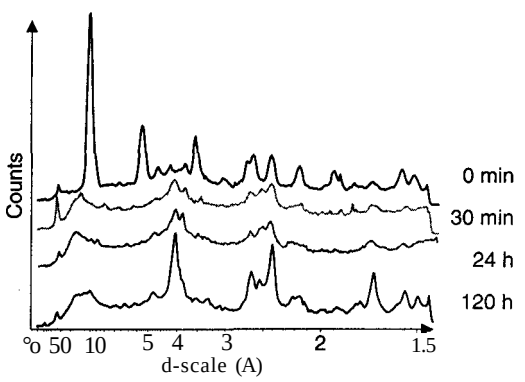

Fig. 2. XRD traces showing $GR_{Na.SO_4}$ transformation after reaction with a high concentration of chromate ($Ox_{Cr(VI)/Fe(II)} = 66\%$) from pure GR (top) to almost pure goethite (bottom). From 1 to 5 days, the peaks narrow, indicating increased grain-size and/or crystallinity with aging. The broad peak with *d*-spacing from 10 to 20 is probably a relic from GR.

In Fig. 3, the pH and Eh curves from a suspension with high Ox_{Cr}(vi)/Fe(ii) are shown. At t — 24 s, chromate is added, and pH drops drastically, but only 6 s later, at t = 30 s, pH has reached a minimum and starts to increase. Eh also responds dramatically upon addition of chromate by increasing 500 mV within a few seconds, but shortly after, it decreases and levels off. These patterns indicate that two separate reactions are taking place simultaneously. The one responsible for the immediate pH drop and Eh increase, is probably oxidation of Fe^{2+} in solution by chromate to an amorphous Cr,Fe-phase. Such a phase is observed in the

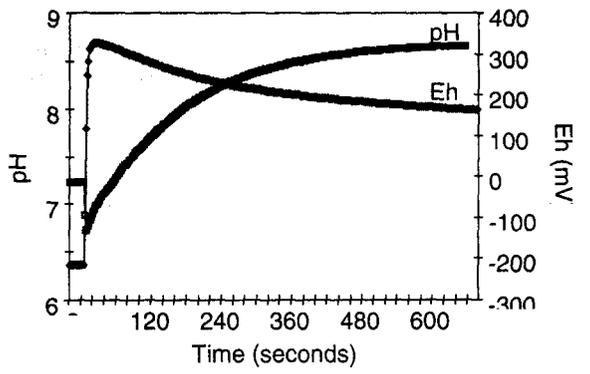

Fig. 3. pH and Eh evolution of a GR_{Na,SO_4} suspension where Cr(VI) was added (relative concentration, $Ox_{Cr(VI)/Fe(II)} = 66\%$). At $t = 24$ s, pH decreases instantly and reaches a minimum after only 6 s where after it increases again. Eh is measured with reference to the standard hydrogen electrode (SHE).

suspension and would be favoured by a rapid reaction. The reaction, which releases protons can be written:

$$\tfrac{1}{4}CrO_4^{2-} + \tfrac{3}{4}Fe^{2+} + 2H_2O = Cr_{0.25}Fe_{0.75}(OH)_{3(am)} + H^+ \quad (2)$$

$Cr_{0.25}Fe_{0.75}(OH)_{3(am)}$ denotes an amorphous Cr,Fe-phase produced stoichiometrically from the reduction of chromate by aqueous iron, but the exact chemical composition of the compound is not known, thus denoted: $Cr_xFe_{1-x}(OH)_{3(am)}$. Table 1 shows that if the concentration of added Cr(VI) is high enough, all aqueous Fe^{2+} is consumed, such as in the case with $Ox_{Cr(VI)/Fe(II)} = 66\%$. In Fig. 3, pH of the solution drops significantly at the instant chromate is added in high proportions, but shortly after, the major reaction of the suspension, i.e., reduction of chromate by GR_{Na,SO_4}, becomes dominant and pH increases:

$$Fe(II)_4Fe(III)_2(OH)_{12}SO_4 \cdot 8H_2O + 4CrO_4^{2-} + 2H^+ = 22Cr_{0.18}Fe_{0.82}OOH + 32H_2O \quad (3)$$

The formula for GR_{Na,SO_4} is written without Na. The exact composition of the Cr-substituted goethite produced from reduction of chromate by GR_{Na,SO_4} is not known ($Cr_xFe_{1-x}OOH$), but is here represented by $Cr_{0.18}Fe_{0.82}OOH$ in order to balance the equation.

The amorphous Cr,Fe-solid is probably identical to the Cr-substituted ferrihydrite described by Loyaux-Lawniczak et al. (1999, 2000). These authors terminated the reaction within 1 min after addition of chromate to GR_{Na,SO_4} and with XRD, Raman and Mössbauer spectroscopy, they identified ferrihydrite, proving the extremely rapid formation. Oxidation of GR_{Na,SO_4} by O_2 leads to different end products, depending on oxidation rate. Hansen (2001) gives the following succession from slow to fast oxidation: Magnetite (Fe_3O_4), goethite (α-FeOOH), lepidocrocite (γ-FeOOH), feroxyhite (δ-FeOOH) and ferrihydrite. Another important factor in controlling the end product is the mechanism of transformation, i.e., whether it is a dissolution–precipitation process or a topotactic transformation process. The oxidising medium also has an influence and so may the treatment of GR prior to reaction. The effect of these parameters can be seen in the spectrum of end products obtained from the previously published studies of Cr(VI) reduction by GR_{SO_4}- Bond and Fendorf (2003) produced a mixture of lepidocrocite and magnetite, Loyaux-Lawniczak et al. (1999, 2000) concluded that their end product after 1 min was ferrihydrite and our experiments produced goethite and ferrihydrite that eventually transformed to goethite. Definition of the parameters controlling the boundaries between the phases would require a dedicated and thorough investigation and is beyond the scope of this work.

In the experiments with very high chromate concentration (Ox_{Cr}(vi)/Fe(ii) = 110%), where more Cr(VI) was present than could be reduced by all of the Fe(II) in GR and solution, XRD shows disruption of the GR structure and the appearance of poorly crystallised goethite (10 min sample). With time, the goethite transformed to a less crystalline phase (Fig. 4). Even after aging for 22 months in the original suspension, in the glove box, this material remained essentially amorphous, as an unidentified phase with two broad peaks at 4.0 A and 3.6 A. The Cr(VI) remaining in solution decreased in concentration with time, probably through association with the Fe(III)-phase. The persistence of the very poorly crystalline phase suggests that abundant Cr(III) destabilises the goethite crystal structure but the coexistence of the Cr(III) and Fe(III) stabilises the mostly amorphous compound.

Others have reported that one of the end products formed during Cr(VI) reduction by GR_{Na,SO_4} is Cr(III)-substituted magnetite (Bond and Fendorf, 2003). We only found magnetite in suspensions where it was present initially, before the addition of chromate. EDS could not detect

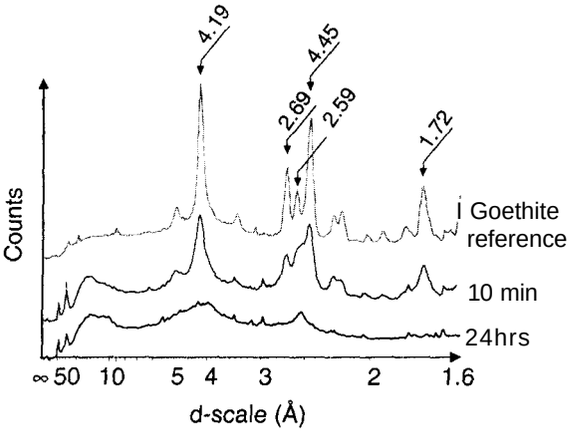

Fig. 4. XRD trace of samples with $Ox_{Cr(VI)/Fe(II)} = 110\%$ (*VH*), where more Cr(VI) is present than can be reduced by Fe(II) in the GR_{Na,SO_4}. The light grey reference trace is from goethite obtained by aerial oxidation of GR_{Na,SO_4}. The dark grey trace represents the data from $VH_{10\,min}$ and clearly shows goethite peaks as well as a poorly crystalline phase with *d*-spacing ranging from 10 to 20 Å, probably a relic from GR. The black trace is from $VH_{24\,h}$. The broad peak at $d = 10$–20 Å resembles that from the transforming GR_{Na,SO_4} and the broad peaks near 4.25 and 2.55 Å remain from goethite, but after a day, the material is mostly amorphous.

Cr associated with magnetite in any samples except the one with high Cr(VI) concentration (Ox_{Cr}(vi)/Fe(ii) = 72%), where a large part of the $GR.N_a,SO_4$ was oxidised. EDS elemental mapping at the nanometer-scale clearly demonstrated that the relatively high concentration of Cr was present only near or at the surface of the magnetite (Fig. 5). This contradicts Bond and Fendorf s conclusion, that magnetite, together with lepidocrocite, governs the fate of Cr reduced by GR_{Na},SO_4 by incorporating Cr(III) in the structure.

3.3. Mechanics of Cr(VI) reduction by GR_{Na,SO_4}

Green rust crystals were morphologically homogeneous in the reaction batches exposed to high Cr(VI) concentrations, but in the lower concentration batches, a variety of crystal morphologies were observed with both AFM and TEM. This larger variety probably arises from very rapid Cr(VI) reduction near the spot where Cr solution enters the suspension, leaving the rest of the GR in the reaction bottle unexposed. Within 10 min of Cr(VI) addition, rims appeared. We define a rim as a zone parallel to the crystal faces, inside the GR crystals (Fig. 6). The original euhedral crystal shape was always preserved and rims were about 50 to 100 nm wide. At medium Cr(VI) concentration (M), the transition zone from rim to core was generally gradual (Fig. 6a), but at high Cr(VI) concentration *(H)*, the rim was separated from the core by a clear band where part of the inner GR crystal had dissolved (Fig. 6b). On AFM images, differences in thickness of the rim, boundary zone and core were obvious (Fig. 6c). At the same time that crystals became zoned, very fine-grained, amorphous Cr,Fe-solid formed in the suspension (Fig. 6b, indicated by the white arrow). The rapid, homogeneous nucleation of this Cr(III)-ferrihydrite suggests easy access of Fe(II) to Cr(VI). The Cr(III), Fe(III) mixed phase probably forms during reaction of dissolved Fe^{2+} with Cr(VI) using GR surfaces as reaction substrate.

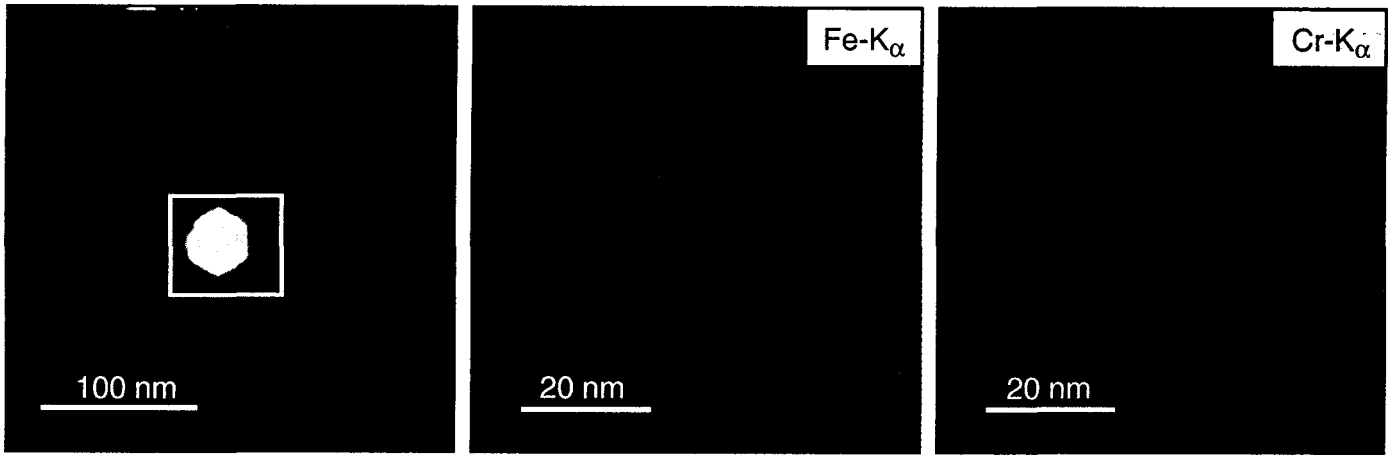

Fig. 5. HAADF-STEM image with EDS elemental maps of a euhedral magnetite crystal (outlined). The maps represent Fe and Cr distribution over the magnetite crystal. The highest counts for Fe are found in the middle of the crystal, whereas the highest counts for Cr are found at the circumference. This demonstrates that Cr is concentrated mainly at the surface of magnetite, not homogeneously incorporated within the magnetite structure.

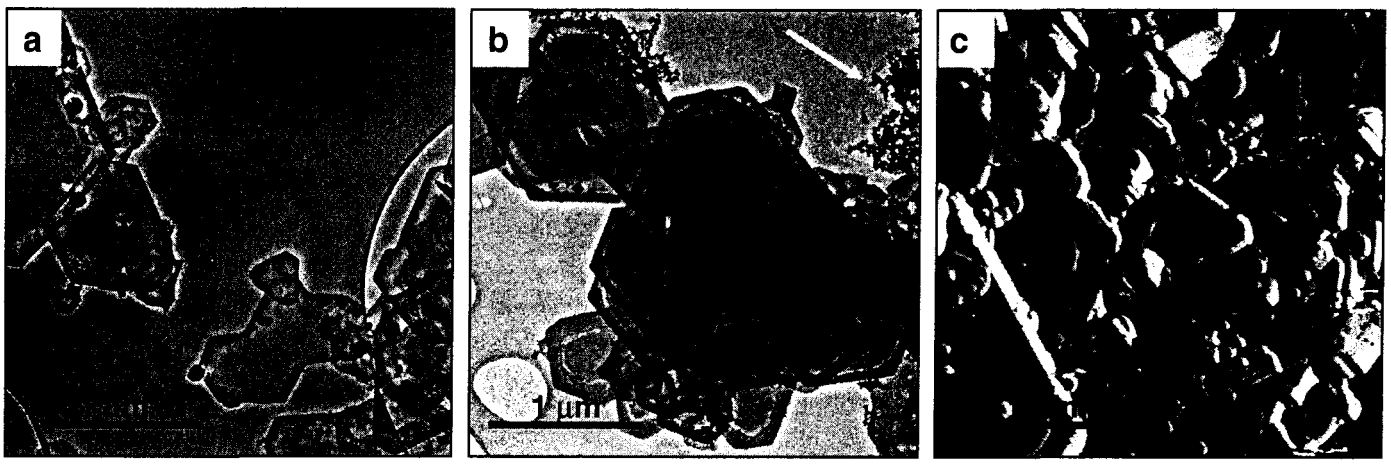

Fig. 6. Images of GR_{Na,SO_4} 10 min after reaction with Cr(VI) (a) BF-TEM image of $Ox_{Cr(VI)/Fe(II)}$ = 35% (*M*), rims are clear on most crystals; (b) BF-TEM image of $Ox_{Cr(VI)/Fe(II)}$ = 72% (*H*), rims and a dissolved band about 100 nm from the edge are visible. A very fine-grained amorphous Cr,Fe-solid (white arrow) has precipitated; (c) AFM image also from *H*($Ox_{Cr(VI)/Fe(II)}$ = 66%) showing the result of dissolution in the boundary region, a band between the rim and core of the crystals.

After equilibrating for more than 20 h, the crystals looked quite different (Fig. 7). The original GR crystal edges have remained sharp, but at high Cr(VI) concentration *(H)*, cores had almost completely dissolved. The samples exposed to Ox_{Cr}(vi)/Fe(ii) = 35% (Af) for 5 days maintained a thicker core (Fig. 7a). At both concentrations, elongated new crystals (about 50 to 100 nm long) were observed inside the relict GR outlines, henceforth called "GR morphs". The new crystallites grew within the rim when Ox_{Cr}(vi)/Fe(ii) = 35% (Fig. 7a) but extended mostly from the rim toward the centre when Ox_{Cr}(vi)/Fe(ii) = 72% (Figs. 7b and c). Consistent with the XRD results, SAED patterns indicated that the new crystals, growing in association with GR morphs, were goethite (data not shown). Semi-quantitative analysis by EDS gave an average Cr concentration of 5% and 9% in crystals from samples in which Ox_{Cr}(vi)/Fe(ii) = 35% and 72%. The amorphous Cr,Fe-solid gradually disappeared as the system equilibrated.

Formation and stabilisation of the new rim texture indicates that GR_{Na,so_4} is oxidised with a different mechanism at the edges than in the core of the crystal. Considering the large space between GR layers, the most probable explanation is diffusion of chromate into the interlayers, as was also suggested by Loyaux-Lawniczak et al. (1999, 2000) and Bond and Fendorf (2003). Chromate, exchanged into the interlayers and most likely replacing sulphate, collects electrons from Fe(II) in close contact. The resulting Fe(III) and Cr(III) are then in place for the formation of Cr-goethite. The structure of GR and goethite are very similar along one crystallographic plane. Thus, an SAED pattern obtained along the c-axis of GR_{Na,so_4} is very close to that obtained for goethite along the a-axis. Hydroxyl, required for the formation of goethite, may form as a result of interlayer water deprotonation and if one or several hydrogens are transferred to oxygen in chromate, only a slight rearrangement of the atoms in the crystal structure is necessary for transition from GR to Cr-goethite. Cr is incorporated into the Fe(III) sites and transformation is essentially topotactic. HR-TEM images (Fig. 8) show that the transformation of $GR_{Na>so_4}$ rims to goethite was gradual and occurred in solid state without dissolution. The thin band between the rim and the core, where material dissolved rapidly, probably results from enhanced solubility at the defects created by the boundary between the two phases.

Cr(III)-goethite is a sparingly soluble compound so its formation blocks further interlayer replacement. The images (Fig. 6) show that reaction rims are less than 100 nm wide, suggesting a limit for Cr transport into the interlayer before goethite formation inhibits further exchange of chromate. New goethite crystals nucleate and grow from the rim. As the amorphous Cr,Fe-solid and the GR core continue to dissolve, more goethite crystals grow towards the core of GR. At high concentration (//), the void in the cores provided plenty of space for formation of goethite crystallites, whereas at medium concentration, GR cores were not dissolved to the same extent. In both samples, discrete goethite crystals frequently precipitate on and near the GR particles (Fig. 7a). Some of these goethite crystallites have the same crystallographic orientation as the goethite that formed within GR or the GR morphs. In other cases, orientation is random, indicating that they nucleated elsewhere.

When Cr(VI) access to the GR interlayer is blocked, remaining Cr(VI) must be reduced at the surface of the remaining GR core. The interlayer space in green rust is composed of cations, anions and a considerable amount of water, providing a pathway for electron transfer across layers from the centre of the GR crystal to the surface. The very rapid reduction (within 10 min) of Cr(VI) while the GR crystals remain essentially intact, is a strong indication for electron transfer across layers. Indeed, experiments with X-ray photoelectron spectroscopy showed that green rust behaves

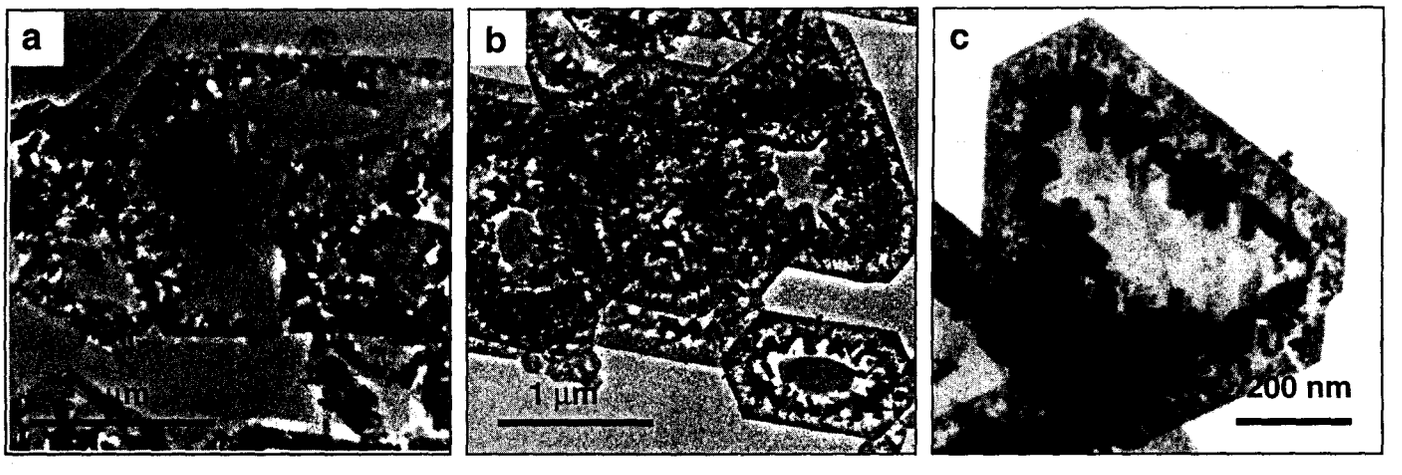

Fig. 7. Particles in suspensions of different Cr concentration *{M* and *H)* after several hours and days of equilibration, observed with TEM. (a) BF-TEM image from Afio days- Goethite grows in the rim of the GR crystals and some goethite rods, with random orientations, have nucleated elsewhere; (b) BF-TEM image from K_2oh» goethite crystals grow from the rims of the GR crystals. The GR cores have mostly dissolved, but in some GR morphs, original GR areas remain, such as in the bottom right corner; (c) HAADF-STEM image with reversed grey-scale from $H_{6\ days}$; the elongated shape of goethite crystals is clearly visible.

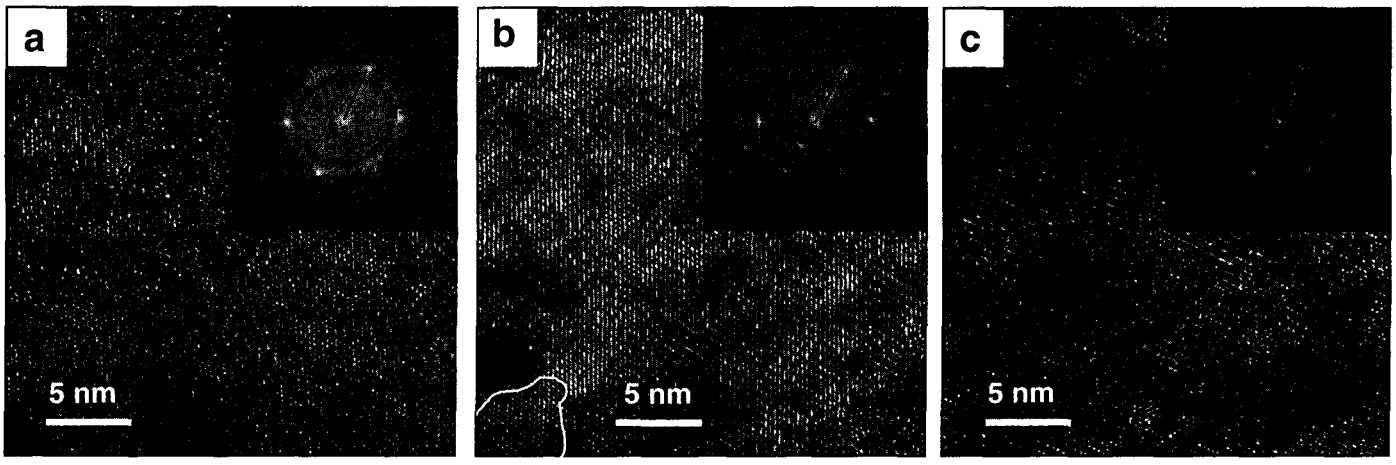

Fig. 8. HR-TEM images of fresh GR and GR transformation morphs. (a) pure GR_{Na,SO_4}, with its Fourier transform (inset); (b) rim of GR morph from suspension $H_{20\,h}$, with double spacing of the lattice fringe. On the FFT (inset), the extra spots, indicating a doubling of the unit cell, are clear. The white line (lower left corner) marks an area that is still GR; (c) from crystals growing inside a GR morph, from suspension $M_{10\ days}$. Double spacing of the lattice fringe is observed in some areas and becomes more pronounced as the equilibration time increases, indicating maturation of the goethite structure.

as a semi-conductor and with scanning tunnelling microscopy (STM), that electrons tunnel in response to a slight potential difference between tip and sample (unpublished results). Yao et al. (1998) have established the possibility for such electron transfer across interlayers for similar layered double hydroxides (LDHs). They were able to tunnel electrons between hydrotalcite crystals on a graphite substrate and a tungsten tip, using STM. Their LDH crystals were 50-70 nm thick, much thicker than those studied here (10-35 nm thick) and hydrotalcite, lacking Fe ions, is bound to have a higher band gap than green rust.

3.4. Implications for reactive barriers

Green rust is effective and fast at reducing dissolved chromate, but in reactive barriers the goals are (1) to optimise accessibility and ensure complete use of the reduced iron capacity, thus minimising cost and maximising barrier life-time, as well as (2) to immobilise Cr, assuring that the fixed Cr will not be released later.

Legrand et al. (2004) investigated the end product of reduction of Cr(VI) by GR_{CO_3} and proposed formation of a surface layer over the reacting GR, which decreases reactivity and increases risk of return to solution. In contrast, the results from the present study on GR_{Na,SO_4}, indicates a different reduction mechanism. Penetration of chromate into the interlayer offers fast access to a portion of the GR_{Na,SO_4} bulk structure and subsequent topotactic transformation to goethite. The Cr-rich amorphous material, produced simultaneously in the initial stages, provides a source of Cr(III) for subsequent precipitation of Cr-goethite. Electron transfer across GR interlayers provides the drive for further reduction until Cr(VI) is used up. It is possible that electron transfer in some GR types is faster than in others.

Contaminants are best immobilised as solid solution in an insoluble mineral rather than adsorbed to particle surfaces. Goethite is only sparingly soluble and with Cr(III) substitution, solubility decreases further. Schwertmann et al. (1989) tested Cr-substituted goethite (7.8 mol% Cr(III)) stability in dissolution experiments with 6 M HCl at 25 °C. The half dissolution time was 660 days for Cr-substituted goethite compared with 8 days for pure goethite. Thus, GR_{Na,SO_4} is not only an effective reducer of Cr(VI), but when GR_{Na,SO_4} is in excess, the Cr(III)-goethite produced is effective at immobilising Cr. When Cr(VI) concentration exceeds the stoichiometric limit defined by the Fe(II) present in the GR, a poorly crystalline Cr(III)–Fe(III)-phase forms that remains stable for many months. Further study would indicate if this material would eventually recrystallise to Cr(III)-goethite in the presence of added GR or if exposure of this poorly crystalline Cr,Fe-phase to ambient conditions would cause later Cr release into the environment.

Acknowledgments

We sincerely thank the other members of the NanoGeoScience group, especially Bo C. Christiansen, for constructive discussion and technical assistance; Frannie Skomurski and Kathy Traexler, University of Michigan for assistance during LLS's visit there; Tonci Balic-Zunic, KU and Hans Christian Bruun Hansen, KVL, Copenhagen for comments on an earlier version of the manuscript; Hanne Nancke-Krogh, KVL; and the technical staff at the Geological Institute, KU, especially Birgit Damgaard, Helene Almind, Peer Jergensen and Vagn Moser. The manuscript was improved by the comments of three anonymous reviewers. The NanoGeoScience Laboratory was established by a grant from the Danish Research Council and the project was supported by contributions from The Swedish Nuclear Waste Management Company (SKB) and the Danish Research Council.

Associate editor: David J. Wesolowski

References

APHA, AWWA, WPCF., 1975. *Standard Methods for the Examination of Water and Wastewater.* American Public Health Association, American Water Works Association and Water Pollution Control Federation, Washington, 14th ed.

Barceloux, D.G., 1999. Chromium. *Clin. Toxicol.* 37 (2), 173-194.

Bernal, J.D., Dasgupta, D.R., Mackay, A.L., 1959. The oxides and hydroxides of iron and their structural inter-relationships. *Clay Mineral Bull.* 4, 15-30.

Bond, D.L., Fendorf, S., 2003. Kinetics and structural constraints of chromate reduction by green rusts. *Environ. Sci. Technol.* 37 (12), 2750-2757.

Christiansen, B.C., Stipp, S.L.S., Balic-Zunic, T., 2004. Improved structural model of green rust sulfate, (GRsoJ- *Geochim. Cosmochim. Ada* **68(11),** A139.

Drits, V.A., Bookin, A.S., 2001. One-dimensional structure models of COj- and SO_4-bearing LDHs. In: Rives, V. (Ed.), *Layered Double Hydroxides: Present and Future.* Nova Science Publishers Inc., New York, pp. 52-92.

Feitknecht, W., Keller, G., 1950. Uber die dunkelgriinen hydroxyverbindungen des eisens. *Zeitschrift fur anorganische chemie* **262,** 61-68.

Gehin, A., Ruby, C, Abdelmoula, M, Benali, O., Ghanbaja, J., Refait, P., Genin, J.-M.R., 2002. Synthesis of Fe(II-III) hydroxysulphate green rust by coprecipitation. *Solid State Sci.* 4, 61-66.

Gibbs, C.R., 1976. Characterization and application of ferrozine iron reagent as a ferrous iron indicator. *Anal. Chem.* 48 (8), 1197-1201.

Hendriksen, P.T., 2003. *Reduktion afnitrat medjern(II)jern(III)hydroxidchlorid : effekt af orthokiselsyre.* M.Sc. thesis at KVL, Copenhagen University, In Danish.

Hansen, H.C.B., Borggaard, O.K., Sorensen, J., 1994. Evaluation of the free energy of formation of Fe(II)-Fe(III) hydroxide-sulphate (green rust) and its reduction of nitrite. *Geochim. Cosmochim. Acta* 58 (12), 2599-2608.

Hansen, H.C.B., 2001. Environmental chemistry of iron(II)-iron(III) LDHs (green rusts). In: Rives, V. (Ed.), *Layered Double Hydroxides: Present and Future.* Nova Science Publishers Inc., New York, pp. **413—** 434.

Koch, C.B., Hansen, H.C.B., 1997. Reduction of nitrate to ammonium by sulphate green rust *Adv. Geoecol.* 30, 373-393.

Lee, W., Batchelor, B., 2002. Abiotic reductive dechlorination of chlorinated ethylenes by iron-bearing soil minerals. 2. Green rust *Environ. Sci. Technol.* **36,** 5348-5354.

Legrand, L., Figuigui, A.E., Mercier, F., Chausse, A., 2004. Reduction ofj; aqueous chromate by Fe(II)/Fe(III) carbonate green rust: kinetic andj| mechanistic studies. *Environ. Sci. Technol.* **38,** 4587^-595.

Lewis, D.G., 1997. Factors influencing the stability and properties of greerit; rusts. *Adv. Geoecol.* 30, 345-372. *t*

Loyaux-Lawniczak, S., Refait, Ph., Ehrhardt, J.-J., Lecomte, P., Genin, J.-M.R., 2000. Trapping of Cr by formation of ferrihydrite during the, • reduction of chromate ions by Fe(II)-Fe(III) hydroxysalt green rusts.! *Environ. Sci. Technol.* 34 (3), 438^43. |:

Loyaux-Lawniczak, S., Refait, Ph., Lecomte, P., Ehrhardt, J.-J., GeninJ i J.-M.R., 1999. The reduction of chromate ions by Fe(II) layered" hydroxides. *Hydrol. Earth Syst. Sci.* 3 (4), 593-599.

Myneni, S.C.B., Tokunaga, T.K., Brown Jr., G.E., 1997. Abiotic selenium redox transformations in the presence of Fe(II,III) oxides. *Science* **278,** 1106-1109.

O'Loughlin, E.J., Kelly, S.D., Cook, R.E., Csencsits, R., Kemner, K.M.,! 2003. Reduction of uranium(VI) by mixed iron(H)/iron(III) hydroxide: (green rust): formation of UO2 nanoparticles. *Environ. Sci. Technol.* 37 : (4), 721-727. •

Pepper, S.E., Bunker, D.J., Bryan, N.D., Livens, F.R., Chamock, J.M., Pattrick, R.A.D., Collison, D., 2003. Treatment of radioactive wastes: an X-ray absorption spectroscopy study of the reaction of technetium with green rust. *J. Colloid Interface Sci.* **268,** 408^12.

Roh, Y., Lee, S.Y., Elless, M.P., 2000. Characterization of corrosion products in the permeable reactive barriers. *Environ. Geol.* 40 (1-2), 184-194.

Schwertmann, U., Gasser, U., Sticher, H., 1989. Chromium-for-iron substitution in synthetic goethites. *Geochim. Cosmochim. Acta* 53, 1293-1297.

Simon, L., Francois, M., Refait, Ph., Renaudin, G., Lelaurain, M., Genin, J.-M.R., 2003. Structure of the Fe(II-III) layered double hydroxysulphate green rust two from Rietveld analysis. *Solid State Sci.* 5 (2), 327-334.

Singer, P.C., Stumm, W., 1970. Acid mine drainage: rate-determining step. *Science* 167(3921), 1121-1123.

Wilkin, R.T., Su, C, Ford, R.G., Paul, C.T., 2005. Chromium-removal processes during groundwater remediation by a zerovalent iron permeable reactive barrier. *Environ. Sci. Technol.* 39, 4599-4605.

Williams, A.G.B., Scherer, M.M., 2001. Kinetics of Cr(VI) reduction by carbonate green rust *Environ. Sci. Technol.* 35 (17), 3488-3494.

Yao, K., Taniguchi, M., Nakata, M., Takahashi, M., Yamagishi, A., 1998. Electrochemical scanning tunneling microscopy observation of ordered surface layers on an anionic clay-modified electrode. *Langmuir* 14, 2890-2895.